tvst

Article

Validation of a Novel Automated Algorithm to Measure Drusen Volume and Area Using Swept Source Optical Coherence Tomography Angiography

Xiaoshuang Jiang[1,2], Mengxi Shen[1], Liang Wang[1], Luis de Sisternes[3], Mary K. Durbin[3], William Feuer[1], Philip J. Rosenfeld[1], and Giovanni Gregori[1]

[1] Department of Ophthalmology, Bascom Palmer Eye Institute, University of Miami Miller School of Medicine, Miami, FL, USA
[2] Department of Ophthalmology, West China Hospital, Sichuan University, Chengdu, China
[3] Research and Development, Carl Zeiss Meditec, Inc., Dublin, CA, USA

Purpose: The purpose of this study was to validate a novel automated swept source optical coherence tomography angiography (SS-OCTA) algorithm to measure elevations of the retinal pigment epithelium (RPE) in eyes with nonexudative age-related macular degeneration (neAMD).

Methods: Patients with drusen were enrolled in a prospective optical coherence tomography (OCT) study and underwent both spectral domain OCT (SD-OCT) and SS-OCTA imaging at the same visit using the 6×6 mm scan patterns. The RPE elevation measurements (square root area and cube root volume) from the SS-OCTA algorithm were compared with the automated validated SD-OCT algorithm on the instrument. Standard deviations of drusen measurements from four repeated scans of another separate set were also calculated to evaluate the reproducibility of the SS-OCTA algorithm.

Results: A total of 53 eyes from 28 patients were scanned on both instruments. A very strong correlation was found between the measurements from the two algorithms (all $r > 0.95$), although the measurements of the drusen area and volume were all larger from the SS-OCTA instrument. The reproducibility of the new SS-OCTA algorithm was analyzed using a sample of 66 eyes from 43 patients. The intraclass correlation coefficient (ICC) was greater than 99% from different macular regions for both the square root area and cube root volume measurements.

Conclusions: A novel automated SS-OCTA algorithm for the quantitative assessment of drusen was validated against the SD-OCT algorithm and was shown to be highly reproducible.

Translational Relevance: This novel SS-OCTA algorithm provides a strategy to measure the area and volume of drusen to assess disease progression in neAMD.

Introduction

Drusen are focal extracellular lipid-rich deposits that accumulate between the basal lamina of the retinal pigment epithelium (RPE) and the inner collagenous layer of the Bruch's membrane (BM) and cause focal elevations of the RPE.[1,2] Large and soft drusen are a distinguishing feature of nonexudative age-related macular degeneration (neAMD), which is the most common cause of legal blindness among the elderly worldwide.[3–10] Drusen are usually characterized by size and shape on color fundus images, and larger drusen have been associated with a higher risk of developing late AMD.[11]

Spectral domain optical coherence tomography (SD-OCT) imaging has been used to generate automated three-dimensional maps of drusen, which provide both area and volume measurements.[12–20] Previously, an automated and validated algorithm has been used to segment the elevated RPE and a "baseline RPE" that approximated the BM layer, also known as RPE-Fit, to generate morphological information on both drusen and other types of RPE elevations, such

translational vision science & technology

as retinal pigment epithelial detachments in exudative AMD, and this information can be used to correlate with disease progression in AMD.[17,21–23] In addition, changes in drusen volume and area measurements have been used in genetic association studies, and complement at-risk alleles have been shown to correlate with drusen size and drusen growth, which may be useful for selecting patients for clinical trials designed to test therapies that could slow drusen growth, cause drusen regression, and slow overall disease progression.[24–26]

The only automated and validated OCT algorithm that is cleared by the US Food and Drug Administration (FDA) and commercially available for the measurement of RPE elevations is found on the Cirrus SD-OCT instrument (Carl Zeiss Meditec, Dublin, CA).[12] This algorithm uses the RPE segmentation to generate a virtual, interpolated "healthy" baseline RPE. The difference between the two segmentations is basically used to identify and measure RPE deformations. Studies have shown that drusen measurements calculated automatically with this algorithm were both highly reproducible and accurate when compared with the manual segmentation of drusen.[15,27] Therefore, when developing a new OCT algorithm for the measurement of RPE elevations using a different instrument, we decided to compare this new algorithm against the previously validated SD-OCT algorithm.

Recently, we developed a new drusen segmentation algorithm for the Plex Elite 9000 swept source optical coherence tomography angiography (SS-OCTA) instrument (Carl Zeiss Meditec, Dublin CA). SS-OCTA utilizes a swept source laser with a longer center point wavelength and faster scanning rates compared with SD-OCT instruments. The new algorithm uses an RPE segmentation essentially equivalent to the one on the Cirrus SD-OCT instrument. However, instead of interpolating a normal RPE layer to create a BM layer, this new algorithm introduces a novel BM segmentation that provides a more anatomically correct "floor" for the drusen measurements. The BM segmentation algorithm uses a new approach, which combines both structure and flow information to determine the location of the BM, and, as a result, it is expected to be more accurate than the previous version. This report describes a validation study performed to compare this new algorithm against the currently available FDA-cleared SD-OCT algorithm.

Methods

Patients were enrolled in a prospective OCT imaging study approved by the institutional review board of the University of Miami Miller School of Medicine, and informed consent was obtained from all the patients. The study was performed in accordance with the tenets of the Declaration of Helsinki and compliant with the Health Insurance Portability and Accountability Act of 1996.

Patients with intermediate AMD (iAMD) underwent both SD-OCT (Cirrus HD-OCT, Carl Zeiss Meditec Inc.) and SS-OCTA (PLEX Elite, Carl Zeiss Meditec Inc.) underwent imaging with both a Cirrus SD-OCT and a PLEX Elite SS-OCTA at the same visit. For our purposes, iAMD was defined as eyes with drusen volume of at least 0.01 mm^3 in the circle of diameter 3 mm centered at the fovea (as measured with the Cirrus HD-OCT). Eyes with other retinal pathologies, including diabetic retinopathy, retinal vein occlusion, central serous chorioretinopathy, and later stage AMD, were excluded from the study. The sample size was determined by the width of the 95% confidence intervals around an intraclass correlation coefficient (ICC) of 0.90 (90%).[28] With a sample size of 40 to 50, we may estimate the ICC with precision ± 0.05.

A 6 × 6 mm scan pattern centered on the fovea was performed on both instruments. The SD-OCT instrument operated at a central wavelength of 840 nm with scanning rate of 68,000 A-scans per second resulting in a full width at half maximum axial resolution of 5 μm in tissue and a transverse resolution of 15 μm estimated at the retinal surface. Eyes were scanned using the SD-OCT instrument using the 200 × 200 macular cube protocol that resulted in the acquisition of a dataset with uniformly spaced A-scans organized as 200 A-scans in each B-scan with 200 horizontal B-scans in each raster array for a spacing between sampling points of 30 μm. The SS-OCTA instrument operated at a central wavelength of 1050 nm with a scanning rate of 100,000 A-scans per second, resulting in a full width at half maximum axial resolution of 6 μm in tissue and a lateral resolution of 20 μm estimated at the retinal surface. Eyes were scanned using the SS-OCTA instrument's angiographic 500 × 500 macular cube protocol that resulted in the acquisition of a dataset with uniformly spaced A-scans organized as 500 A-scans in each B-scan with each B-scan repeated twice at each position and 500 horizontal B-scan positions in each raster array for a spacing between sampling points of 12 μm. A different set of eyes were selected for the test-retest repeatability portion of the study to assess the SS-OCTA algorithm. Each one of these eyes was imaged four times during a single session.

For the SD-OCT scans, the validated Advanced RPE Analysis software that was available on the instrument was used to calculate the drusen area and volume in the 3 mm and 5 mm circles centered on the fovea.

Table. Comparison of Drusen Measurements Between SD-OCT and SS-OCTA Algorithms

	Square Root Area (3 mm Circle) Mean $\pm$ SD (mm)	Square Root Area (5 mm Circle) Mean $\pm$ SD (mm)	Cube Root Volume (3 mm Circle) Mean $\pm$ SD (mm)	Cube Root Volume (5 mm Circle) Mean $\pm$ SD (mm)
SD-OCT	1.17 $\pm$ 0.40	1.28 $\pm$ 0.51	0.41 $\pm$ 0.13	0.42 $\pm$ 0.15
SS-OCTA	1.39 $\pm$ 0.41	1.54 $\pm$ 0.55	0.47 $\pm$ 0.14	0.49 $\pm$ 0.15
P value	<0.001	<0.001	<0.001	<0.001

Abbreviations: SD: standard deviation, SD-OCT: Spectral Domain Optical Coherence Tomography, SS-OCTA: Swept Source Optical Coherence Tomography Angiography.
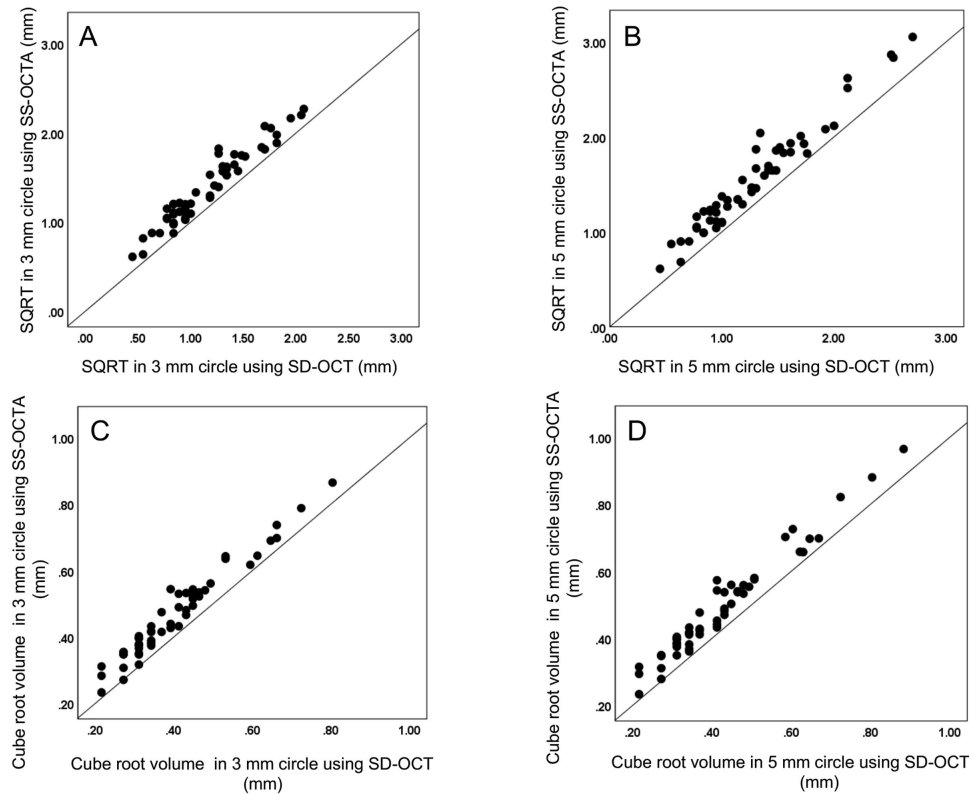

Figure 1. Comparison of drusen measurements between spectral domain OCT (SD-OCT) and swept source OCT (SS-OCTA) algorithms. (**A**) Square root (SQRT) of drusen area using SD-OCT versus SS-OCTA in 3 mm circle, $r = 0.94$. (**B**) SQRT of drusen area using SD-OCT versus SS-OCTA in 5 mm circle, $r = 0.96$. (**C**) Cube root of drusen volume using SD-OCT versus SS-OCTA in 3 mm circle, $r = 0.96$. (**D**) Cube root of drusen volume using SD-OCT versus SS-OCTA in 5 mm circle, $r = 0.96$. Solid line is the line of unity with a slope = 1.

For the SS-OCTA scans, the unprocessed OCT datasets were exported from the instrument and uploaded to the Advanced Retina Imaging (ARI) Network on the ARI Network Hub (https://arinetworkhub.com) provided by Carl Zeiss Meditec. Drusen area and volume measurements were calculated using version 0.10 of the Advanced RPE Analysis algorithm. This algorithm is a prototype implementation that will be included on a future release of the commercial instrument. The algorithm output provided quantitative values for drusen area and volume in the 3 mm and 5 mm circles centered at the fovea. In both the SD-OCT and SS-OCTA, the foveal position is automatically determined by a proprietary algorithm and reported in terms of X and Y coordinates based on pixel position within the scans. Square root transformation of area measurements and cube root transformation of volume measurements were performed to eliminate the impact of lesion size on the variability of the standard deviation (SD) previously determined from test-retest measurements. The advantages provided by these transformations have been established in previous studies.[12]

Paired sample *t*-tests were performed to detect differences in the square root of drusen area measurements and the cube root of the drusen volume measurements between the SD-OCT and SS-OCTA algorithms. Bland-Altman plots were used to illustrate the mean difference between the square root drusen area and cube root drusen volume measurements obtained from
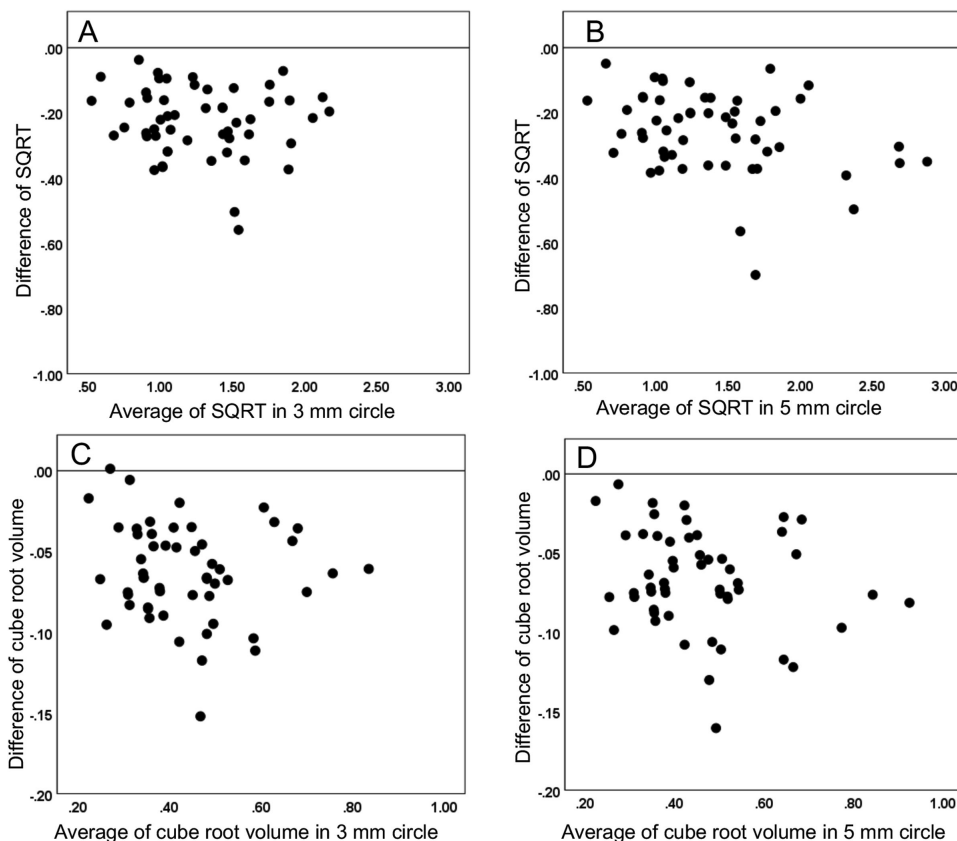
Figure 2. Bland Altman plots of drusen measurements between two algorithms for the mean differences of the square root (SQRT) area and cube root volume measurements versus the average measurements obtained using the spectral domain OCT (SD-OCT) and swept source OCT (SS-OCTA) algorithms in the 3 mm and 5 mm circles centered on the fovea. (**A**) SQRT of drusen area in the center 3 mm circle. (**B**) SQRT of drusen area in the center 5 mm circle. (**C**) Cube root of drusen volume in the center 3 mm circle. (**D**) Cube root of drusen volume in the center 5 mm circle.

the two algorithms. Reproducibility of the SS-OCTA algorithm was assessed with the ICC for the square root of the drusen area and cube root of drusen volume measurements from the different regions. A higher ICC indicates better reproducibility of the parameter. The test-retest SDs of each set of measurements were calculated for each eye and plotted versus the mean measurements. All *P* values of < 0.05 were considered clinically significant. All statistical analysis was performed using IBM SPSS Statistics for Windows, version 25.0 (IBM Corporation, Armonk, NY).

Results

The square root of the drusen area and the cube root of drusen volume measurements were compared between the SD-OCT and SS-OCTA algorithms. The total sample of 53 eyes included 36 eyes from 19 women and 17 eyes from 9 men, with a mean age of 70.9 ± 5.7 years (range = 60–85).

Generally, the measurements for the drusen area and volume from SS-OCTA were larger than those from SD-OCT. In the center 3 mm circle, the mean drusen area measurements were 1.52 mm^2 and 2.11 mm^2 from the SD-OCT and SS-OCTA scans, respectively, and the mean square root of the drusen area measurements were 1.17 mm and 1.39 mm from the SD-OCT and SS-OCTA scans, respectively. In the 5 mm circle, the mean drusen area measurements were 1.89 mm^2 and 2.67 mm^2 from the SD-OCT and SS-OCTA scans, respectively, and the mean square root of drusen area measurements were 1.28 mm and 1.54 mm from the SD-OCT and SS-OCTA scans, respectively. Similarly, the cube root drusen volumes were larger from the SS-OCTA scans. In the center 3 mm circle, the mean drusen volume measurements were 0.09 mm^3 and 0.13 mm^3 from the SD-OCT and SS-OCTA scans, respectively, and the mean cube root of drusen volume measurements were 0.41 mm and 0.47 mm from the SD-OCT and SS-OCTA scans, respectively. In the center 5 mm circle, the mean drusen volume measurements were 0.11 mm^3 and 0.16 mm^3
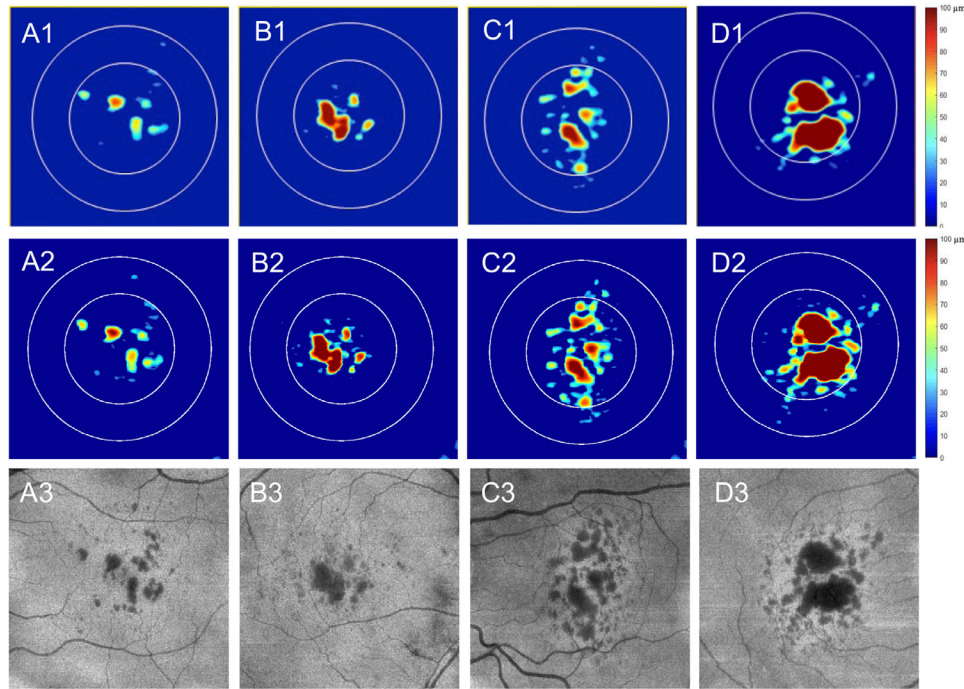
Figure 3. Drusen elevation maps showing similar measurements in the 3 mm and 5 mm circles obtained from the same patients imaged using the spectral domain OCT (SD-OCT) and swept source OCTA (SS-OCTA) instruments. (**A1**, **B1**, **C1,** and **D1**) The drusen elevation maps generated from the SD-OCT Advanced RPE Analysis algorithm. (**A2**, **B2**, **C2**, and **D2**) The drusen elevation maps generated from the SS-OCTA Advanced RPE Analysis algorithm from the same patients. (**A3**, **B3**, **C3**, and **D3**) Represent the en face structural maps obtained directly from the SS-OCTA instrument when using a segmentation slab with boundaries between the retinal pigment epithelial layer and the RPE-fit layer.
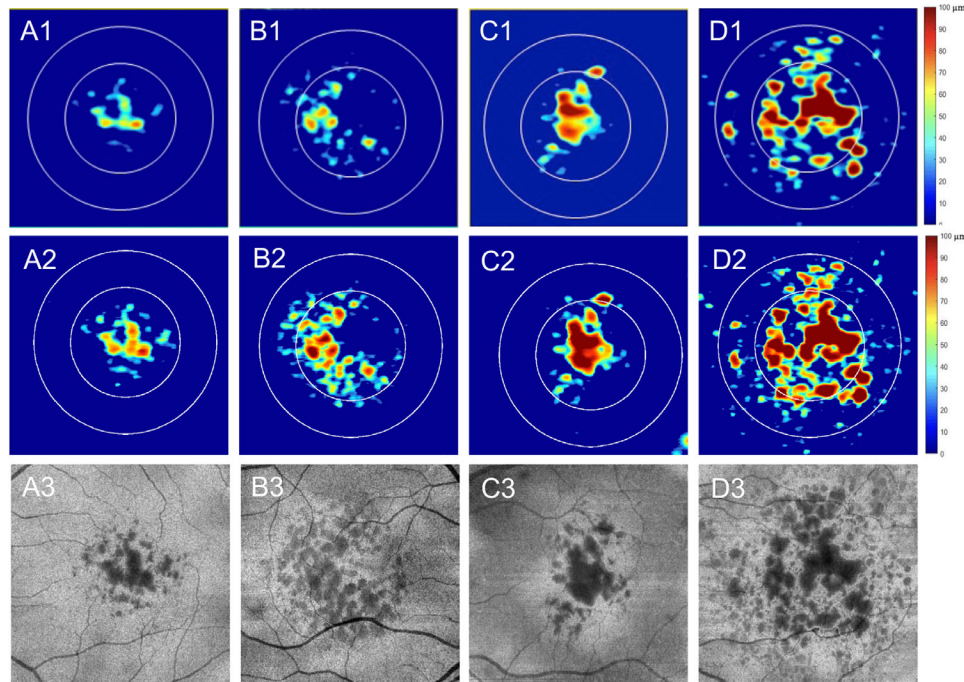

Figure 4. Drusen elevation maps showing slightly different measurements in the 3 mm and 5 mm circles obtained from the same patients imaged using the spectral domain OCT (SD-OCT) and swept source OCTA (SS-OCTA) instruments. (**A1**, **B1**, **C1**, and **D1**) The drusen elevation maps generated from the SD-OCT Advanced RPE Analysis algorithm. (**A2**, **B2**, **C2**, and **D2**) The drusen elevation maps generated from the SS-OCTA Advanced RPE Analysis algorithm from the same patients. (**A3**, **B3**, **C3**, and **D3**) Represent the structural maps obtained directly from the SS-OCTA instrument when using a segmentation slab with boundaries between the retinal pigment epithelial layer and the RPE-fit layer.

from the SD-OCT and SS-OCTA scans, respectively, and the mean cube root drusen volume measurements were 0.42 mm and 0.49 mm from SD-OCT and SS-OCTA scans, respectively. The differences between the square root and cube root measurements from these two instruments were significantly different both in the center 3 mm and 5 mm circles (all $P < 0.0001$, paired t-test; Table). However, there were extremely strong correlations between the measurements obtained with the two algorithms. The correlation coefficients were 0.96 and 0.98 for the square root of drusen area in the 3 mm and 5 mm circles, and the correlation coefficients were 0.98 and 0.98 for the cube root of drusen volume measurements in the 3 mm circles and the 5 mm circles. All the correlations were highly statistically significant ($P < 0.001$; Fig. 1).

Bland-Altman plots (Fig. 2) clearly indicate a systematic difference in measurements between the SD-OCT and SS-OCTA algorithms in which the SS-OCTA measurements are larger than the SD-OCT, and this difference is substantially independent of the drusen burden. Figure 3 shows drusen elevation maps in eyes with increasing drusen area and volume and relatively small measurement differences. Figure 4 shows drusen elevation maps in eyes where the SS-OCTA algorithm detected relatively larger area and volume measurements compared with the SD-OCT algorithm. Figure 5 demonstrates the reason for the larger area and volume measurements obtained from the SS-OCTA algorithm. As shown in this figure, the new BM segmentation from the ARI network's advanced RPE analysis version 0.10 algorithm more accurately followed the anatomic BM and there is no overlap between the segmentation lines corresponding to the RPE and the BM in the SS-OCTA algorithm, whereas the lines overlap slightly, as seen in the valleys between the drusen in the SD-OCT algorithm. Thus, the SS-OCTA algorithm appears to provide a more accurate segmentation for the calculation of drusen area and volume measurements, which explains the systematic differences between the two measurements in which the SS-OCTA measurements are larger.

We also studied the test-retest repeatability of the new RPE elevation algorithm using four repeated OCT scans obtained at the same visit. For this purpose, we used a separate sample of 66 eyes from 43 patients, including 45 eyes from 29 women and 21 eyes from 14 men, with a mean age of 72.2 ± 5.7 years (range = 60.4–86.3).

Both the qualitative appearance of the drusen maps and quantitative measurements of the square root area and cube root volume had excellent repeatability. Figure 6 shows mean of the square root drusen area and cube root drusen volume measurements and
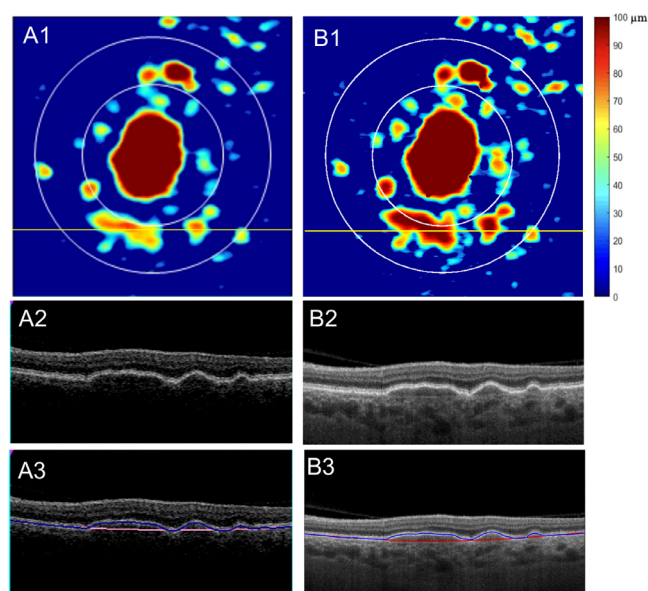

Figure 5. Drusen elevation maps with B-scans and segmentation lines depicting the retinal pigment epithelium (RPE) and Bruch's membrane (BM) using algorithms developed for the spectral domain OCT (SD-OCT) and swept source OCTA (SS-OCTA) scans. (**A1**) The drusen elevation map generated from the SD-OCT algorithm. (**B1**) The drusen elevation map generated from the SS-OCTA algorithm. (**A2** and **B2**) The B-scans corresponding to the horizontal yellow lines in **A1** and **B1**. (**A3** and **B3**) The blue lines correspond to the RPE segmentation line and the red lines correspond to the BM segmentation line using the different algorithms.

their SDs for the 3 mm circle, 5 mm circle, and the total scan area. Both the square root drusen area and cube root drusen volume measurements were highly reproducible. The ICC for the 4 repeat scans was more than 99% in different regions for both the square root and cube root measurements, similar or better than the reproducibility of the SD-OCT scans.[12,29] Moreover, the SDs were small in comparison to the means over the entire range of measurements. There was no significant correlation between the SDs and mean measurements of the square root of area and cube root of volume between repeated scans using the SS-OCTA algorithm. It should be noted that repeatability depends on both the RPE/Bruch segmentations and the algorithm that locates the foveal center. For instance, the large outlier shown by the arrow in Figures 6A and 6D, was analyzed in detail in Figures 7I to P. This outlier was caused by an incorrect foveal position, as shown in Figure 7L. Once the foveal position was edited manually and the data re-analyzed, the SD of the drusen measurements for the four repeated scans from this eye decreased drastically (Fig. 8).
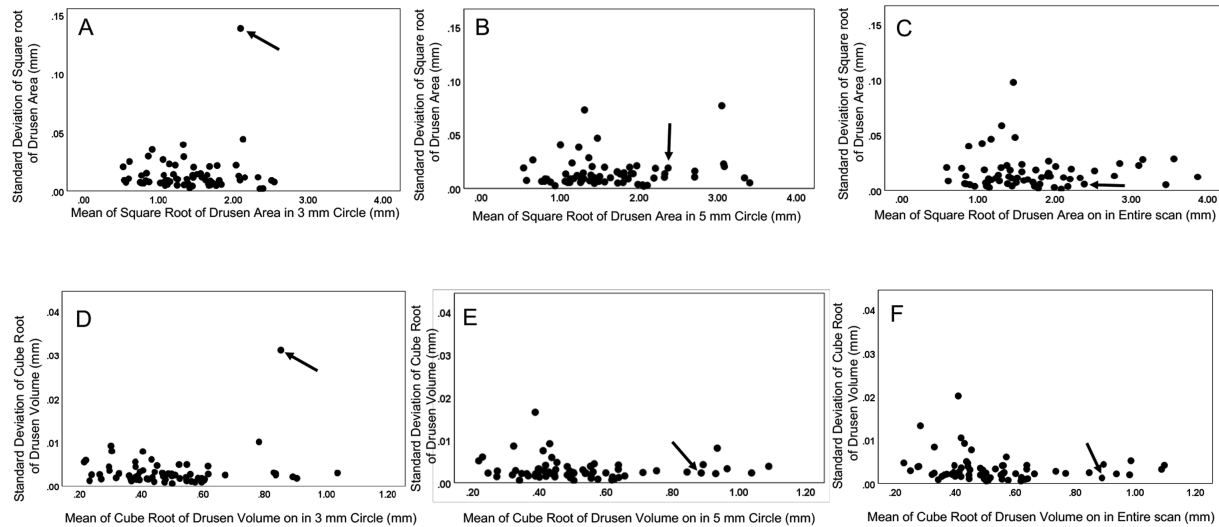
Figure 6. Relationship between the standard deviation and the mean of the square root area and cube root volume measurements using the swept source OCTA (SS-OCTA) algorithm. (**A** and **D**) The 3 mm circle. (**B** and **E**) The 5 mm circle. (**C** and **F**) The entire scan. The outliner identified by the black arrow show a relatively large variance in the 3 mm circle but not in the 5 mm circle and in the entire scan. Figure 7 explains the basis for this variance.

Discussion

Quantitative measurements characterizing the health of the RPE and, in particular, the drusen burden can clearly play an important role in better understanding different pathologies and the effects of treatment. A number of different approaches have been proposed to produce automated drusen burden measurements from OCT datasets,[12,18–20,30–32] including a few recent algorithms involving aspects of convolutional neural networks.[30–32] Although it is difficult to compare precisely the performance of the different algorithms in the literature, at this time, the RPE elevation algorithm commercially available on the Cirrus SD-OCT instrument is clearly the best understood and most widely used one. In this study, we evaluated the performance of a novel automated RPE elevation algorithm developed for the Plex Elite SS-OCTA instrument by comparing drusen volume and area measurements to those obtained using the algorithm on the Cirrus SD-OCT instrument, which is the only RPE elevation algorithm cleared by the FDA. Furthermore, we analyzed the repeatability of the new algorithm using four scans of the same eye. Excellent agreement between the two algorithms was demonstrated, with the SS-OCTA algorithm yielding slightly higher values due to a more accurate segmentation of the BM anatomic layer. The interclass agreement for the SS-OCTA algorithm was more than 99% for both the square root area and cube

root volume measurements, establishing a remarkable reproducibility similar to that of the Cirrus algorithm. Therefore, we can conclude that the new automated SS-OCTA algorithm performs very well, producing drusen area and volume measurements that are intrinsically consistent with, and somewhat more accurate than, those obtained using the current gold-standard algorithm.[12,15,16,21,27]

This new SS-OCTA algorithm improves upon the current SD-OCT algorithm by introducing an actual BM segmentation that provides a more anatomically correct "floor" for the drusen measurements. The BM segmentation algorithm uses a novel approach that combines both structure and flow information to determine the location of the BM. Although the details of the proprietary, commercial algorithm studied here cannot be fully disclosed, a recent paper from Schottenhamml et al.[33] appeared in the literature after this work had been submitted. It describes a Bruch's segmentation algorithm based on the same principles. In the SD-OCT algorithm, the BM was identified instead using a virtual RPE interpolation that at times can have a tendency to ride above the actual BM position along the B-scan,[12,27] particularly in the presence of large confluent drusen or RPE detachments, where the RPE is interpolated over extended regions. Furthermore, in order to reduce the effects of "noise" due to a certain lack of consistency in the location of the interpolated drusen floor in eyes with different geometries, a relatively higher threshold is needed to identify drusen, leading to a tendency to undercount small
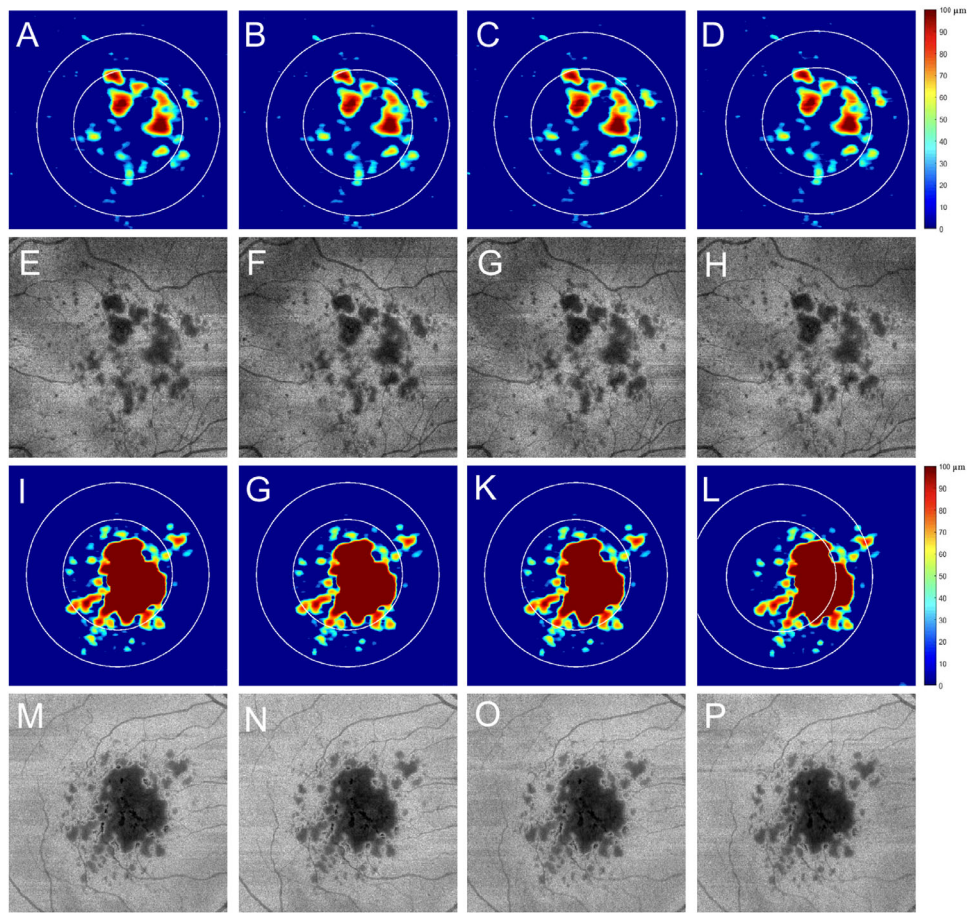
Figure 7. Repeated drusen elevation maps depicting the both small and large variances in the volume and area measurements using the swept source OCTA (SS-OCTA) algorithm. (**A**, **B**, **C**, and **D**) The drusen elevation maps with excellent repeatability from four scans. (**E**, **F**, **G**, and **H**) The en face drusen structural maps using the retinal pigment epithelium (RPE) and RPE-fit segmentation boundaries off the instrument and corresponding to panels **A**, **B**, **C**, and **D**. (**I**, **G**, **K**, and **L**) The drusen elevation maps with panel **L** showing a shift of the 3 mm and 5 mm circles relative to panels **I**, **G**, and **K**. (**M**, **N**, **O**, and **P**) The en face drusen structural maps using the retinal pigment epithelium (RPE) and RPE-fit segmentation boundaries off the instrument and corresponding to panels **I**, **G**, **K**, and **L**.

drusen, as illustrated in Figure 4. Although contributions from other factors, including intrinsic differences between SD-OCT and SS-OCTA datasets that cannot be completely discounted, this explains the major differences between the algorithms. In general, the drusen elevation maps generated using the SS-OCTA algorithm appear to follow the true drusen morphology somewhat more closely and therefore can be expected to produce more accurate measurements. However, it is worth pointing out explicitly that the strength of the new algorithm (i.e. a BM segmentation taking advantage of the blood flow information available in OCTA scans), also makes it less generally applicable, as it cannot be used on purely structural scans.

Despite the difference between the algorithms in the segmentation of BM, there was still excellent consistency between the SD-OCT and SS-OCTA algorithms even with the technical differences in the acquisition of the images. Although both the SD-OCT and SS-OCTA scan patterns were isotropic with equal spacing between A-scans and B-scans, the SD-OCT 200 × 200 scan pattern had 30 μm spacing between sample points, whereas the SS-OCTA 500 × 500 scan pattern had a spacing of 12 μm, which also has the potential to result in more accurate quantitation of RPE elevations. The use of denser scans, may also contribute to the improved performance of the new algorithm in detecting small drusen that were often missed by the SD-OCT algorithm (see Fig. 4).

Both algorithms do a good job of segmenting drusen and we did not see any large segmentation errors in our sample. However, we did not attempt to carry out a careful analysis of possible errors, as our purpose was to compare the results of the two automated algorithms without any corrections and/or modifications. Nevertheless, it should be mentioned
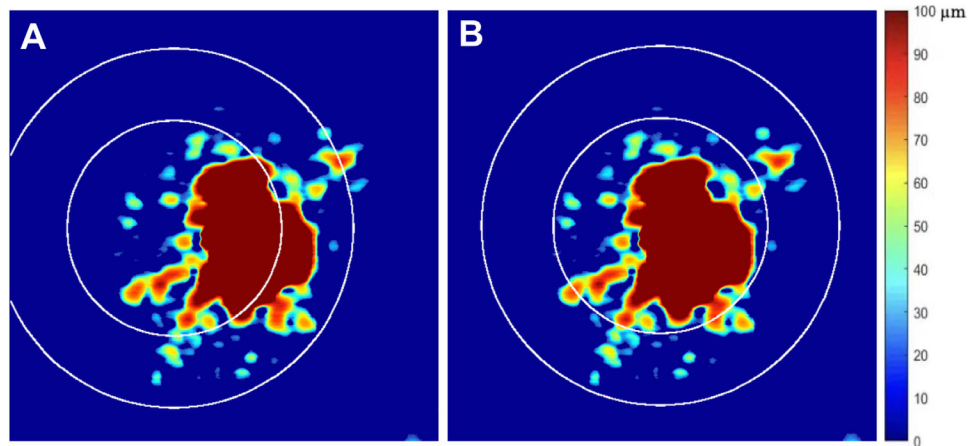
Figure 8. Drusen elevation maps before and after manually editing the position of the foveal center location in the swept source OCTA (SS-OCTA) algorithm. (**A**) Represents an offset of the 3 mm and 5 mm circles based on an incorrect foveal location. (**B**) The drusen elevation map and corresponding circles once the foveal position was manually edited in the SS-OCTA algorithm.

that a potential source of variability in drusen measurements is the automated post-acquisition macular foveal location algorithm. Our previous study showed that automated algorithm in SD-OCT designed to detect the foveal center was more accurate than the fixation target of the instrument and the automated foveal center was close to the manually detected foveal center with a shift of approximately 3 to 6 pixel in drusen eyes.[34] Usually, the foveal detection algorithm is quite reliable, however, when we checked a large outlier in the SD of the repeated measurements we found that it was an eye with a large drusenoid retinal pigment epithelium detachment (PED) whose drusen maps are shown in Figures 7I to L. In this example, the automated foveal detection was shifted in one of the scans (see Fig. 7L), compared with the other three repeats. The incorrect foveal offset led to an artificially large SD for the center 3 mm circle, as shown by the arrow in Figures 6A and 6D. Interestingly, this shift only affected the quantitation in the center 3 mm circle and not the 5 mm circle because the drusenoid PED was fully contained within the 5 mm circle. If exact quantitation is needed in a given area, it is important to remember that the foveal position should be checked, especially in the setting of large PEDs, and manually corrected if necessary. In any case, the algorithm to outline RPE elevations is independent of the fovea position, so the fovea position can be checked visually on the en face images and anatomically using B-scans, and, if incorrect, it can be corrected to produce more accurate measurements within the 3 mm and 5 mm circles.

The limitations of our study include a relatively small sample size, even though the comparisons were highly statistically correlated. Although we included a wide range of drusen sizes, we only assessed RPE elevations in eyes with neAMD, whereas other types of PEDs in exudative AMD complicated by both intraretinal fluid and subretinal fluid were not assessed and will be evaluated in future studies. Although the current SS-OCTA algorithm is not commercially available, it is undergoing FDA-clearance and will be available in future software updates of the PLEX Elite 9000 SS-OCTA operating software. Despite these limitations, this novel SS-OCTA algorithm for the detection of RPE elevations should provide a convenient, repeatable, accurate strategy to reliably measure the area and volume of drusen and other types of PEDs.

Acknowledgments

References

1. Curcio CA. Soft drusen in age-related macular degeneration: biology and targeting via the oil spill strategies. *Invest Ophthalmol Vis Sci.* 2018;59(4):160–181.

2. Chen L, Messinger JD, Sloan KR, et al. Abundance and multimodal visibility of soft drusen in early age-related macular degeneration: a clinicopathologic correlation. *Retina.* 2020;40(8):1644–1648.

3. Abdelsalam A, Del Priore L, Zarbin MA. Drusen in age-related macular degeneration: pathogenesis, natural course, and laser photocoagulation-induced regression. *Surv Ophthalmol.* 1999;44(1):1–29.

4. Schlanitz FG, Ahlers C, Sacu S, et al. Performance of drusen detection by spectral-domain optical coherence tomography. *Invest Ophthalmol Vis Sci.* 2010;51(12):6715–6721.

5. Pauleikhoff D, Barondes MJ, Minassian D, Chisholm IH, Bird AC. Drusen as risk factors in age-related macular disease. *Am J Ophthalmol.* 1990;109(1):38–43.

6. Bressler SB, Maguire MG, Bressler NM, Fine SL. Relationship of drusen and abnormalities of the retinal pigment epithelium to the prognosis of neovascular macular degeneration. The Macular Photocoagulation Study Group. *Arch Ophthalmol.* 1990;108(10):1442–1447.

7. Davis MD, Gangnon RE, Lee LY, et al. The Age-Related Eye Disease Study severity scale for age-related macular degeneration: AREDS Report No. 17. *Arch Ophthalmol.* 2005;123(11):1484–1498.

8. van Leeuwen R, Klaver CC, Vingerling JR, Hofman A, de Jong PT. The risk and natural course of age-related maculopathy: follow-up at 6 1/2 years in the Rotterdam study. *Arch Ophthalmol.* 2003;121(4):519–526.

9. Wang JJ, Foran S, Smith W, Mitchell P. Risk of age-related macular degeneration in eyes with macular drusen or hyperpigmentation: the Blue Mountains Eye Study cohort. *Arch Ophthalmol.* 2003;121(5):658–663.

10. Klein R, Klein BE, Knudtson MD, Meuer SM, Swift M, Gangnon RE. Fifteen-year cumulative incidence of age-related macular degeneration: the Beaver Dam Eye Study. *Ophthalmology.* 2007;114(2):253–262.

11. Ferris FL, 3rd, Wilkinson CP, Bird A, et al. Clinical classification of age-related macular degeneration. *Ophthalmology.* 2013;120(4):844–851.

12. Gregori G, Wang F, Rosenfeld PJ, et al. Spectral domain optical coherence tomography imaging of drusen in nonexudative age-related macular degeneration. *Ophthalmology.* 2011;118(7):1373–1379.

13. Alexandre de Amorim Garcia Filho C, Yehoshua Z, Gregori G, Farah ME, Feuer W, Rosenfeld PJ. Spectral-domain optical coherence tomography imaging of drusenoid pigment epithelial detachments. *Retina.* 2013;33(8):1558–1566.

14. Diniz B, Ribeiro R, Heussen FM, Maia M, Sadda S. Drusen measurements comparison by fundus photograph manual delineation versus optical coherence tomography retinal pigment epithelial segmentation automated analysis. *Retina.* 2014;34(1):55–62.

15. Gregori G, Yehoshua Z, Garcia Filho CA, et al. Change in drusen area over time compared using spectral-domain optical coherence tomography and color fundus imaging. *Invest Ophthalmol Vis Sci.* 2014;55(11):7662–7668.

16. Yehoshua Z, Gregori G, Sadda SR, et al. Comparison of drusen area detected by spectral domain optical coherence tomography and color fundus imaging. *Invest Ophthalmol Vis Sci.* 2013;54(4):2429–2434.

17. Yehoshua Z, Wang F, Rosenfeld PJ, Penha FM, Feuer WJ, Gregori G. Natural history of drusen morphology in age-related macular degeneration using spectral domain optical coherence tomography. *Ophthalmology.* 2011;118(12):2434–2441.

18. Chiu SJ, Izatt JA, O'Connell RV, Winter KP, Toth CA, Farsiu S. Validated automatic segmentation of AMD pathology including drusen and geographic atrophy in SD-OCT images. *Invest Ophthalmol Vis Sci.* 2012;53(1):53–61.

19. Chen Q, Leng T, Zheng L, et al. Automated drusen segmentation and quantification in SD-OCT images. *Med Image Anal.* 2013;17(8):1058–1072.

20. Jain N, Farsiu S, Khanifar AA, et al. Quantitative comparison of drusen segmented on SD-OCT versus drusen delineated on color fundus photographs. *Invest Ophthalmol Vis Sci.* 2010;51(10):4875–4883.

21. Penha FM, Rosenfeld PJ, Gregori G, et al. Quantitative imaging of retinal pigment epithelial detachments using spectral-domain optical coherence tomography. *Am J Ophthalmol.* 2012;153(3):515–523.

22. de Amorim Garcia Filho CA, Penha FM, Gregori G, Rosenfeld PJ. Increasing volume of a retinal

pigmented epithelial detachment as a predictor of submacular hemorrhage during anti-VEGF therapy. *Ophthalmic Surg Lasers Imaging Retina.* 2013;44(2):204–207.

23. Penha FM, Gregori G, Garcia Filho CA, Yehoshua Z, Feuer WJ, Rosenfeld PJ. Quantitative changes in retinal pigment epithelial detachments as a predictor for retreatment with anti-VEGF therapy. *Retina.* 2013;33(3):459–466.

24. Chavali VR, Diniz B, Huang J, Ying GS, Sadda SR, Stambolian D. Association of OCT derived drusen measurements with AMD associated-genotypic SNPs in Amish population. *J Clin Med.* 2015;4(2):304–317.

25. Garcia Filho CA, Yehoshua Z, Gregori G, et al. Change in drusen volume as a novel clinical trial endpoint for the study of complement inhibition in age-related macular degeneration. *Ophthalmic Surg Lasers Imaging Retina.* 2014;45(1):18–31.

26. Schaal KB, Rosenfeld PJ, Gregori G, Yehoshua Z, Feuer WJ. Anatomic clinical trial endpoints for nonexudative age-related macular degeneration. *Ophthalmology.* 2016;123(5):1060–1079.

27. Nittala MG, Ruiz-Garcia H, Sadda SR. Accuracy and reproducibility of automated drusen segmentation in eyes with non-neovascular age-related macular degeneration. *Invest Ophthalmol Vis Sci.* 2012;53(13):8319–8324.

28. Fleiss JL. *The Design and Analysis of Clinical Experiments.* New York, NY: Wiley & Sons; 1986.

29. de Sisternes L, Jonna G, Greven MA, Chen Q, Leng T, Rubin DL. Individual drusen segmen-tation and repeatability and reproducibility of their automated quantification in optical coherence tomography images. *Transl Vis Sci Technol.* 2017;6(1):12.

30. Khalid S, Akram MU, Hassan T, Jameel A, Khalil T. Automated segmentation and quantification of drusen in fundus and optical coherence tomography images for detection of ARMD. *J Digit Imaging.* 2018;31(4):464–476.

31. Mishra Z, Ganegoda A, Selicha J, Wang Z, Sadda SR, Hu Z. Automated retinal layer segmentation using graph-based algorithm incorporating deep-learning-derived information. *Sci Rep.* 2020;10(1):9541.

32. Waldstein SM, Vogl WD, Bogunovic H, Sadeghipour A, Riedl S, Schmidt-Erfurth U. Characterization of drusen and hyperreflective foci as biomarkers for disease progression in age-related macular degeneration using artificial intelligence in optical coherence tomography. *JAMA Ophthalmol.* 2020;138(7):740–747.

33. Schottenhamml J, Moult EM, Ploner SB, et al. OCT-OCTA segmentation: combining structural and blood flow information to segment Bruch's membrane. *Biomed Opt Express.* 2021;12(1):84–99.

34. Wang F, Gregori G, Rosenfeld PJ, Lujan BJ, Durbin MK, Bagherinia H. Automated detection of the foveal center improves SD-OCT measurements of central retinal thickness. *Ophthalmic Surg Lasers Imaging.* 2012;43(6 Suppl):S32–S37.

translational vision science & technology